Spatiotemporal phase synchronization in adaptive reconfiguration from action observation network to mentalizing network for understanding other's action intention

Li Zhang[1], John Q. Gan[2,3], Wenming Zheng[2] and Haixian Wang[2,*]

[1]School of Medical Imaging, Bengbu Medical College, Bengbu, Anhui 233030, PR China

[2]Research Center for Learning Science, Southeast University, Nanjing, Jiangsu 210096, PR China

[3]School of Computer Science and Electronic Engineering, University of Essex, Colchester CO4 3SQ, UK

Correspondence:
Prof. Haixian Wang
Research Center for Learning Science
Southeast University
2 Sipailou Road
Nanjing, Jiangsu 210096, China
Email: hxwang@seu.edu.cn

Abstract

In action intention understanding, the mirror system is involved in perception-action matching process and the mentalizing system underlies higher-level intention inference. By analyzing the dynamic functional connectivity (DFC) in α (8-12Hz) and β (12-30Hz) frequency bands over a "hand-cup interaction" observation task, this study investigates the topological transition from the action observation network (AON) to the mentalizing network (MZN), and estimates their functional relevance for intention identification from other's different action kinematics.

Sequential brain microstates were extracted based on event-related potentials (ERPs), in which significantly differing neuronal responses were found in N170-P200 related to perceptually matching kinematic profiles and P400-700 involved in goal inference. Inter-electrode weighted phase lag index (WPLI) analysis on the ERP microstates revealed a shift of hub centrality salient in α frequency band, from the AON dominated by left-lateral frontal-premotor-temporal and temporal-parietooccipital synchronizations to the MZN consisting of more bilateral frontal-parietal and temporal-parietal synchronizations.

As compared with usual actions, intention identification of unintelligible actions induces weaker synchronizations in the AON but dramatically increased connectivity in right frontal-temporal-parietal regions of the MZN, indicating a spatiotemporally complementary effect between the functional network configurations involved in mirror and mentalizing processes. Perceptual processing in observing usual/unintelligible actions decreases/increases requirements for intention inference, which would induce less/greater functional network reorganization on the way to mentalization. From the comparison, our study suggests that the adaptive topological changes from the AON to the MZN indicate implicit causal association between the mirror and mentalizing systems for decoding others' intentionality.

Keywords: action intention understanding; ERP brain microstate; dynamic functional connectivity; action observation network; mentalizing network

1 Introduction

Understanding others' goals and motives underlying their actions is crucial for communication between individuals who live in the social world. From others' distinct patterns of kinematics, action intentions may be distinguished via direct perception or via inferential processes, which are thought to rely on the mirror system, *i.e.,* action observation network (AON), mapping visual information onto the motor representation in our memory of our own actions, or the mentalizing system enabling us to extract and understand others' goals, thoughts, and beliefs by drawing on "social intelligence" (Becchio et al. 2012; Brass et al. 2007; Catmur 2015; Liew et al. 2011; Rizzolatti et al. 2001; Van Overwalle and Baetens 2009; Woodward and Gerson 2014).

Through low-level perceptual input, the mirror system might result in direct awareness of the goal of a perceived action, by recognizing what is being done and how an action is being performed, especially for familiar or frequently executed actions (Buccino et al. 2004; Decety and Grèzes 1999; Rizzolatti et al. 2007; Van Overwalle and Baetens 2009). At a higher level of understanding why an action is being performed, mirror neurons might respond to acquire actor's immediate intention, on condition that there is contextual information or a specific chain of motor acts (Carter et al. 2011; Catmur 2014, 2015; Ortigue et al. 2009; Woodward and Gerson 2014). While in the absence of contextual information or observing unusual actions, the mentalizing system might be particularly recruited to fill in the "missing" information, by use of the inferential processes to judge others' mental states (Blakemore and Decety 2001; Becchio et al. 2012; Brass et al. 2007; Catmur 2015; Liew et al. 2011; Van Overwalle and Baetens 2009; Spunt et al. 2011).

Brain imaging studies have demonstrated that both mirror neurons and mentalizing areas are involved in action intention understanding. Perception of action kinematics might be an initial stage in the identification of others' intentions, followed by the recruitment of inferential processes or other cognitive functions (Becchio et al. 2012; Blakemore and Decety 2001; Catmur 2015; Virji-Babul et al. 2010; Van Overwalle 2009). However, the transition from mirror to mentalizing system and the conditions in which each dominates need to be explored (Becchio et al. 2012; Van Overwalle and Baetens 2009; Tidoni and Candidi 2016). Moreover, functional relevance between mirror matching and inferential processes is still unclear and hotly debated, especially the role of AON in inferring the goal of an observed action (Becchio et al. 2012; Catmur 2015; Marsh et al. 2014; Neal and Kilner 2010; Tidoni and Candidi 2016). Some studies argue that the mirror system and the mentalizing system are largely mutually independent of each other, because they are rarely concurrently activated in action intention understanding tasks (Van Overwalle and Baetens 2009; Virji-Babul et al. 2010). A number of studies suggest that the AON may support inferential process by providing sensorimotor information to mentalizing areas for making correct inferences about others' intentions. Nevertheless, more causal evidence is needed to reveal how these two systems may cooperate and inform each other (Catmur 2015; Gardner et al. 2015; Tidoni and Candidi 2016).

Recent dynamic network research has provided new insight into dynamic fluctuations in the brain network structure related to ongoing cognitive function and the process of replacing one routing function with another while the network keeps running (Hutchison et al. 2013). Specifically, the topological reorganization of the functional brain network has been found to be modulated by cognitive load and individual's mental effort, *i.e.,* engaged proportion of the total amount of cognitive resources needed to complete a task (Bassett et al. 2006; Kitzbichler et al. 2011). The mentalizng system activation shows the load-dependent increase, in particular, during social cognitive information processing (Meyer et al. 2012; Spunt et al. 2013). Thus, in this study we assume that the perceived visual information in action observation process imposes different cognitive loads on an observer during higher-level goal inference, which probably modulates functional integration among brain areas in the mentalizing network (MZN).

Using a "hand-cup interaction" observation task, dynamic functional connectivity (DFC), *i.e.*, functional connectivity changing over a short time, was investigated in this study to estimate the evolving and interconnected nature in the transition from the AON to the MZN. To test the interactive relationship between the two functional networks, the DFC of observing actions performed in an intention-oriented usual way was compared with that in a non-intentional unintelligible way, since the two types of actions have different cognitive demands in mirror matching and intention inference processes. Technically, the timing and localization of mirror responses and mentalization were determined by event-related potential (ERP) and source trace, and the DFC of functional brain networks in the time intervals of ERP components was measured by computing phase synchronization and evaluated according to graph theory. After that, identifiable spatiotemporal EEG features were identified for recognizing different types of action intentions. According to the DFC changing over the task course, the conditions under which the AON is dominated or interrupted by the MZN, and functional relevance between the topological organizations of AON and MZN were analyzed and discussed.

2 Materials and Methods

2.1 Participants

This study recruited 30 college students from Southeast University to participate in the EEG experiment. Exclusion criteria of subjects included left handedness, medical, neurological, or psychiatric illness, and history of brain injury or surgery. After excluding the data seriously contaminated by noise, artifacts or movements, effective data of 24 subjects composed of 10 males and 14 females aged 22.4±2.3 (mean±SD) were retained and analyzed. The study was approved by the Academic Committee of the Research Center for Learning Science, Southeast University, China. All the subjects were asked to read and sign a fully informed consent form for this experiment and received payment for their participation.

2.2 Experimental paradigm

In this experiment, all the participants were asked to view three "hand-cup interaction" actions performed by a person, which were recorded as stationary frames, including two typical intention-oriented actions, rather usual in normal life, and a non-intentional action unintelligible to normal observers. The task was adapted from that designed in the study of Ortigue et al. (2009). All the stimuli were presented in the E-prime 2.0 procedure.

Fig. 1A illustrates the three actions in "no context" condition: 1) Use grip (Ug): a right hand is grasping a cup for the purpose of using it; 2) Transport grip (Tg): a right hand is grasping a cup for the purpose of moving it; 3) Simple contact (Sc): a right hand is touching a cup without a clear purpose.

The experimental task includes a "Ug" condition, a "Tg" condition, and an "Sc" condition. Each condition consists of 98 trials, resulting in 294 trials in total. In each task condition, the performer's hand motions were the same across trials, but the cup was randomly marked with one of 7 standard colors with equal probability, so each color was repeatedly used 14 times. The trials from "Ug", "Tg" and "Sc" conditions were cross-presented with a pseudorandom probability. Consecutive presentation of the same hand motion was preset as less than 4 times, and the same constrain was set for the presentation of cups with the same color.

The time for each subject to conduct the experiment was about 24 minutes. The stimuli were presented sequentially along the timeline illustrated in Fig. 1. The presentation order and duration are shown in Fig. 1B. After the symbol "+" at the center of screen presented for 150 ms, a cup was shown for 500 ms. Then a hand interacted with the cup appeared on the screen for 2000 ms. When the hand-cup interaction action was presented, subjects were asked to judge the intention of the actor, which was supposed to be conducted just in their brains without pressing any button. Before the onset of the next trial, the symbol "+" was shown again with a random time length ranging from 1000 ms to 2000 ms as the inter-trial interval. Before the formal experiment, a practice session including 12 trials was conducted by each subject, in which each hand motion was repeatedly presented 4 times.

2.3 EEG recording and preprocessing

The EEG data were recorded by the Neuroscan international 10-20 system with a sampling rate of 500 Hz, using 60 electrodes covering frontal, parietal, temporal, and occipital regions. Additionally, two reference electrodes were placed on the bilateral mastoids of subjects, and four surface electrodes simultaneously recording electrooculographic (EOG) signals were used to monitor ocular movements and eye blinks, with one pair placed over the higher and lower left eyelids and the other pair placed 1 cm lateral to the outer corner of the left and right orbits.

The raw EEG data were then preprocessed by the Scan 4.3 software. The continuous signals were band-pass filtered within a frequency band range of 1-60 Hz. Each trial was further extracted within a time window of 1200 ms, including 200 ms for the pre-stimulus period and 1000 ms for the post-stimulus period. The time point dividing pre- and post- stimuli is the onset of hand-cup interaction action along the timeline of stimulus presentation (Fig. 1B). The baseline correction was performed following the pre-stimulus time interval and ocular artifacts were removed according to the simultaneously recorded EOG signals. After the artifact rejection with thresholds ranging from 50 μv to 75 μv, the trials contaminated by eye blinks and electrocardiogram noise were excluded. Furthermore, the independent component analysis (ICA) plugged in the EEGLAB toolbox was conducted to clear visible artifacts, such as the components of ocular and muscle movements (Delorme and Makeig 2004).

The EEG data across subjects from the three conditions were divided into "Ug", "Tg", and "Sc" groups, consisting of 1146, 1174, 1139 trials respectively, of which 36~68 trials were retained under each condition for each subject.

2.4 ERP brain microstate analysis and source estimation

To dissociate the cognitive brain states involved in the action intention understanding task, we used ERPs and difference waveforms to establish the time course during which the processes of mirror matching and intention inference occur instantaneously. The ERPs were found being elicited in different action intention discrimination tasks, within which neural responses to the observed actions significantly differ as an indicator of visual perception and goal inference (Ortigue et al. 2009, 2010; Van Overwalle et al. 2009; Van der Cruyssen et al. 2009; Vistoli et al. 2015).

Sequential ERP microstates: Firstly, a micro-segmentation of standard ERP components was conducted to construct sequential stable microstates with representative configuration of global electric potential (Cacioppo et al. 2014; Khanna et al. 2015). A microstate refers to momentary, patterned, and quasi-stable global functional state of the brain, and reflects a time-limited information processing operation (Koenig et al. 2002). Event-related brain microstates can reflect different cognitive functions, such as perception, attention, disease, emotion, and reasoning (Milz et al. 2016). For the data from each task condition, an averaged ERP file across all the trials and subjects was created. The ERP waveform can be represented as a $T \times n$ matrix with T being the number of timeframes and n the number of EEG channels. The averaged ERP data were processed by using the Chicago Electro-Neuroimaging Analytics (CENA) toolbox (Cacioppo et al. 2014; Cacioppo and Cacioppo 2015). Unlike the traditional methods for extracting microstate topology, such as k-means clustering method, the CENA performs a data-driven (automatic) detection of non-periodic quasi-stable brain states through parsing the ERPs into the baseline state, stable microstates, and non-stable transitions between these states. The micro-segmentation by the CENA tool was conducted in four major steps: 1) Root mean square error (RMSE) metric was computed for identifying the transitions across discrete microstates; 2) Global field power (GFP) was estimated to discover the changes in the overall level of brain activation; 3) Based on cosine distance between the template maps derived from the 60-dimensional sensor space for successive evoked microstates, similarity metric was computed to confirm whether the microstates identified in terms of the RMSE differ in the configuration of brain activity; 4) Bootstrapping procedure was performed for identifying heterogeneities in the timing or number of microstates as well as their representative template maps across subjects.

Difference wave analysis: Secondly, a "difference waveform" between ERPs was computed to isolate the components of interest, since difference wave was thought to represent psychological processes that are different between two conditions. In this study, difference wave configuration was created between 60-dimensional ERPs by subtracting the ERP waveform elicited by one condition from the ERP waveform elicited by another, and topological maps of difference waveforms with GFP peaks were constructed for every pair of task conditions to test within-subject effect on brain states.

Cortical source estimation: Finally, the cortical source of every stable microstate was estimated by using a cortical source estimation procedure implemented in the Brainstorm toolbox (http://neuroimage.usc.edu/brainstorm; Tadel et al. 2011), and the source current of difference waveform was estimated as well. The EEG signals were assumed to be generated from a block of electric dipoles at the cortical surface. The forward model was calculated with a symmetric Boundary Element Model (BEM) in OpenMEEG, an open-source software (http://www-sop.inria.fr/athena/software/OpenMEEG/; Gramfort et al. 2010), on the cortical surface of a template MNI brain ("Colin27" atlas), with a 1 mm resolution. Specifically, the noise of the scalp sensors was removed through computing the noise covariance matrix of the signals in the pre-stimulus time interval. Cortical sources were estimated by means of an inverse kernel matrix that had been produced by the forward model and the standardized Low Resolution Brain Electromagnetic Tomography (sLORETA) estimation algorithm. After that, the cortical sources were mapped to a distributed source model consisting of 15,002 elementary current dipoles.

2.5 WPLI analysis and construction of functional microstate networks

To investigate how action perception and intention inference modulate local specialization and inter-regional integration in the brain, functional networks of event-related oscillations were constructed in the temporal windows of ERPs. It has been suggested that true interaction between two neural sources results in a coherent phase relationship between their corresponding time series, which is represented by a value ranging from 0 and π (Vinck et al. 2011).

Inter-trial coherence of principle components: The assessment of functional connectivity is based on an analysis of phase synchrony between pairwise EEG signals in α (8-12Hz) and β (12-20Hz) frequency bands. The frequency selection was determined by an inter-trial coherence (ITC) analysis for the principle components located at left and right cerebral hemispheres, because ITC can statistically detect the time-frequency regions with event-related phase-locking events for all trials in a dataset (Delorme and Makeig 2004) (Fig. 2).

Association matrix of phase synchronization: Centering around the time point of the GFP peak of each ERP component, consecutive functional microstate networks were constructed with the 60 EEG channels used as the nodes. The length of each time window of a microstate network is at least 100 ms, to ensure that at least one cycle is available for estimating phase relationship between neural signals in α and β frequency bands. It is well-known that volume conduction can cause spurious increase of connectivity between sensors. In order to reduce sensitivity to additional and uncorrelated noise sources and increase statistical power in detecting true changes in phase synchronization, weighted phase lag index (WPLI) (Vinck et al. 2011) was used to measure the existence of time-lagged interdependence between two time series of EEG signals.

The basic idea of phase lag index (PLI) is to investigate the asymmetry of the distribution of phase differences around zero, which is given by

$$PLI = |\langle sign(\Delta\emptyset_{rel}(t))\rangle| = \left|\frac{1}{X}\sum_{x=1}^{X} sign(\Delta\emptyset_{rel}(t_x))\right|$$

where $\Delta\emptyset_{rel}$ is phase difference at time-point x between two time series, which is determined for all time-points ($x = 1 \dots X$) per time window, $sign$ stands for signum function, < > denotes the operation of mean value, and | | indicates the absolute value. Instantaneous phases were determined by the Hilbert transformation, applying a Hanning window on the concurrent fast Fourier transform. The range of the PLI value is $[0,1]$, with 0 denoting no coupling or coupling with a phase difference centered around 0 mod π and 1 representing perfect phase locking at the values of $\Delta\emptyset_{rel}(t)$ different from 0 mod π. Although PLI shows robustness against the presence of common sources, *i.e.*, volume conduction and the possibly active reference in EEG, it is biased and loses some ability to detect changes in phase synchronization of noisy signals, especially in the case of weak coupling (Vinck et al. 2011).

As a weighted version of PLI, WPLI has been recently developed to tackle the problems of small-magnitude synchronization effect existing in PLI. WPLI weights each phase difference according to the magnitude of the imaginary component of the cross-spectrum, therefore, phase differences around zero only marginally contribute to the calculation of WPLI. Since the contribution of the observed phase leads and lags is weighted, WPLI presents "reduced sensitivity to uncorrelated noise sources and increased statistical power to detect changes in phase synchronization (PS)" (Vinck et al. 2011).

Through computing WPLI for each pair of EEG time series averaged across trials for each task condition and for each subject, sequential 60×60 association matrices were created for the brain microstates changed over the task course.

Undirected network construction: For each association matrix, an adjacent matrix was acquired through applying a threshold by the following steps: 1) In the pre-stimulus period, a fixed connection density p was set abiding by the Erdös-Rényi model (1961) for each subject (*i.e.*, $p = 2\ln n/n$, where n is the number of the nodes, *i.e.*, channels), to get a no-task WPLI adjacency matrix; 2) the minimum WPLIs of all the pre-stimulus adjacency matrices from the 24 subjects were averaged; 3) The mean was then used as a fixed threshold to be applied to all the association matrices of the microstates in the post-stimulus period, to acquire task-related WPLI adjacent matrices. With these adjacent matrices, sequential undirected graphs along the time course were constructed for further connectivity analysis.

2.6 Functional connectivity and network topology metrics of sequential graphs

To assess the DFC of the brain network, the global structure and local node characteristic of the sequential graphs were measured according to graph theory (Bullmore and Sporns 2009; Rubinov and Sporns 2010). Global integration of a functional network was estimated by using connection density and characteristic path length. While assessing local specialization of a functional brain network, we focused on a particular type of graph-based method that identifies the nodes that play central roles within the network structure. Specifically, centrality measures make implicit assumptions about the manner in which traffic flows through a network (Lohmann et al. 2010; Opsahl et al. 2010; Sporns et al. 2007). According to the suggestion of Sporns *et al.* (2007), a combination of various graph measures, named "node centrality", was employed here to characterize such nodes, including degree, betweenness and closeness centrality.

According to the definitions from graph theory, N is the set of all the nodes in a network and (i, j) represents the edge between nodes i and $(i, j \in N; i \neq j)$. If there is connection status between nodes i and j, $a_{ij} = 1$; otherwise, $a_{ij} = 0$. The following graph metrics can be estimated based on the connectivity matrix defined by a_{ij}.

Connection density: It refers to the number of edges in a graph comprising n nodes divided by the maximum number of possible edges $[(n^2 - n)/2]$.

Characteristic path length: It is the average number of edges in the shortest paths between all the nodes, *i.e.*,

$$L = \frac{1}{n}\sum_{i \in N} L_i = \frac{1}{n}\sum_{i \in N} \frac{\sum_{j \in N, j \neq i} d_{ij}}{n-1}$$

where L_i is the average distance between node i and other nodes, and $d_{ij} = \sum_{a_{uv} \in g_{i \to j}} a_{uv}$ refers to the shortest path length between nodes i and j ($g_{i \to j}$ is the shortest geodesic path between i and j). For all the disconnected node pairs i and j, $d_{ij} = \infty$.

Node connection strength: It refers to the sum of weights attached to ties belonging to a node in a weighted network. In this study, connection strength of node i is given by the sum of the WPLIs of the adjacent edges connected to the node.

$$s_i = \sum_{j \in N} a_{ij} w_{ij}$$

where w_{ij} is the WPLI between node i and node j.

In the following computations for the three measurements of node centrality, edge weights were added to the graph that roughly correspond to the length of the paths, which had been calculated using the Euclidean distance between the coordinates of the end nodes of each edge.

Degree centrality: Node degree is the most fundamental network measure, which is quantified by the number of connections linked to node i:

$$k_i = \sum_{j \in N} a_{ij}$$

A node with high degree centrality is viewed as a "pivotal hub" in a network.

Closeness centrality: The closeness centrality of node i is calculated as the inverse of the average distance from this node to all other nodes in the network (*i.e.,* the inverse of the row mean of the distance matrix):

$$C_i = \frac{n-1}{\sum_{j \in N} d_{ij}}$$

Closeness centrality measures how many steps, on average, a node takes to reach everyone else in the network. Thus, the distance from a node with high closeness centrality to any other node is short on average. These nodes are considered to be structurally important, because they can easily reach or be reached by others.

Betweenness centrality: It is measured based on the proportion of the number of the shortest paths between all node pairs, which pass through a specific node, to the total number of shortest paths between all node pairs. The measurement can assess the communication role of the node within the functional network. It is defined as follows:

$$b_i = \frac{1}{(n-1)(n-2)} \sum_{\substack{h,j \in N \\ h \neq j, h \neq i, j \neq i}} \frac{\rho_{hj}(i)}{\rho_{hj}}$$

where ρ_{hj} is the number of the shortest paths between nodes h and j, and $\rho_{hj}(i)$ is the number of the shortest paths between nodes h and j that pass through node i. Nodes with high betweenness centrality are crucial to play the role of "connector hub" in a network.

2.7 Statistical and discriminate analyses of differences between action intentions

Using the 24 subjects as the testing samples, the amplitudes of ERPs from 60 channels elicited by different task conditions were statistically tested by the paired Student's t-tests. Additionally, to detect the systematic differences in functional connectivity of α- and β-band phase-synchronized networks, the graph-theoretical measurements of global topology and local nodes between every two conditions were statistically compared by the paired Student's t-tests. A false discovery rate (FDR) procedure was used to correct for multiple hypothesis testing, with significance level set to 0.05. The null hypothesis is that there is no difference between task conditions.

For α- and β-band functional networks, connection strengths of each EEG electrode were extracted in the temporal windows of N170-P200 and P400-700 responses to constitute two-dimensional input features for the discriminant analysis between task conditions. Then the subject-based feature samples were recognized using linear discriminant analysis (LDA), support vector machine (SVM) and Naive Bayes individually, to find the distinguishable electrode sites from the time-varying functional connectivity microstates in identifying other's different action intentions.

3 Results

3.1 Time-locked ERP brain microstates and source localization

The grand average of ERPs from EEG midline electrodes in "Ug", "Tg", and "Sc" conditions are shown in Fig. 3. It can be found that N70, P120, N170-P200, P300 and P400-700 are elicited by the three conditions. Specifically, the disassociations among the three ongoing waveforms can be found in representative electrodes FZ, CZ, PZ and POZ.

Corresponding to the ERPs, continuous brain microstates were constructed for each task condition by parsing the series of electric potential configurations. Fig. 4 illustrates the temporal evolution of microstate topologies, in which five stable microstates under "Ug" condition were retrieved by the CENA procedure after excluding transition states with too short duration. Each topological map and source distribution correspond to the global potential peak of a representative ERP component. For "Tg" and "Sc" conditions, topological maps and source distributions can be constructed similarly. The durations and cortical sources of the five event-related microstates are summarized in Table 1.

Statistical analysis has revealed the EEG electrode distribution with significant disassociations in the ERPs of microstates 2~5, in which the N170-P200 microstate has been particularly found having the maximum number of electrodes with significant potential difference between "Ug" and "Sc" and between "Ug" and "Tg" conditions (paired Student's t-tests with FDR correction: $p<0.05$) (Fig. 5C and 5E). The difference waves of N170-P200 are consistently located in left cerebral hemisphere, involving the premotor cortex, inferior frontal gyrus (IFG), anterior intraparietal sulcus (IPS), superior temporal sulcus (STS) and posterior parietooccipital cortices. However, there are no significant potential differences in N170-P200 waves in the EEG electrodes between "Tg" and "Sc" conditions (paired Student's t-test with FDR correction, $p>0.05$) (Fig. 5D). On the other hand, the P400-700 microstate also shows high sensitivity to different action intentions. The brain mapping and source analysis for GFP peaks reveal that the maximum currents in P400-700 are distributed at the medial prefrontal cortex (mPFC), anterior cingulate cortex (ACC), and right temporo-parietal junction (TPJ) (Fig. 4 and Fig. 5B). As shown in Fig. 3, there is remarkable differentiation in P400-700 waves among the three conditions, in which "Sc" condition particularly evokes the highest response amplitude. While compared with "Ug" and "Tg" conditions, difference waves from "Sc" condition are manifested as higher local field potential activities in the mPFC, right IFG, STS, and anterior temporal lobe but less responses in left temporal lobe and posterior parietal-occipital areas (paired Student's t-test with FDR correction, $p<0.05$) (Fig. 5C and 5D).

3.2 Event-related phase-synchronized networks over task course

Under the three action intention conditions, the phase-synchronized networks constructed based on the continuous time-locked ERPs are presented in Fig. 6. It can be seen that understanding usual and unintelligible actions generates different levels of event-related functional connectivity and topological reorganization.

Especially at the time intervals with N170-P200 evoked, *i.e.*, the duration of microstate 3, functional connections in α- and β-band networks focus on the frontal, premotor, temporal, parietal and occipital areas in left-lateral cerebral hemisphere. Specifically, there are dense inter-regional phase synchronizations for understanding usual actions in "Ug" and "Tg" conditions. As a contrast, the functional network of N170-P200 shaped under "Sc" condition shows the most sparse connections in both α and β frequency bands, reflecting suppressed synchronized activities for inter-regional information transmission (Fig. 6A and 6B). While in the later phase with P400-700 evoked, *i.e.*, the duration of microstate 5, the networks are mainly composed of functional connections distributed in left-lateral frontal-temporal and bilateral parietal-occipital areas. Right frontal and temporal areas are differentially involved in the three task conditions. Especially in "Sc" condition, there are strongly increased synchronized activities among prefrontal, inferior frontal, parietal and temporal areas in right cerebral hemisphere, which is more salient in the α-band functional network (Fig. 6A).

3.3 Effect of tasks on spatiotemporal evolution of functional connectivity

The graph-theoretical analysis reveals the temporal evolution of global topology of functional brain networks. As shown in Fig. 7A and 7B, following the ERP-indexed cognitive microstates, global connection density of α- and β-band event-related networks tends to increase gradually, while characteristic path length shows a tendency of decrease. The timeline of global network measurements implies that the cognitive processing in the later phases (microstates 4~5) recruits more connections and so induces strongly enhanced global integration in the networks, which subserves strengthened functional connectivity and global efficiency of information transmission. While compared with "Ug" and "Tg" conditions, the functional network topology in "Sc" condition shows the lowest global connection density and the highest characteristic path length in the early phase (statistical significance is partly found in paired Student's t-tests on α- and β-band networks: $p<0.05$; Fig. 7A and 7B), but it is organized in an almost reversed way in the later phase, *i.e.*, the highest connection density and the lowest path length (statistical significance is partly found in paired Student's t-tests on α-band networks: $p<0.05$; Fig. 7A), which denotes the greatest adaptive reconfiguration of functional brain networks in the transition from the earlier to the later cognitive sub-processes in understanding other's unintelligible action intention. Besides, there are no significant differences in global topological measurements between the networks shaped in "Ug" and "Tg" conditions.

The analysis of local nodes has revealed a shift of hub centrality following the topological reorganization of the event-related networks. Especially in the α-band networks derived from N70, P120 and N170-P200 components, it can be found that the pivotal hubs with relatively high "degree" centrality scores focus on left central, temporal, parietal and occipital areas. However, in the α-band networks corresponding to P300 and P400-700 responses, the most pivotal hubs are distributed in right-lateral posterior brain areas and inferior frontal lobe. Some nodes in right prefrontal cortex (PFC) are particularly involved in "Sc" condition (Fig. 8A). Apart from the changes of node degree distribution, α-band networks show local reorganization in the nodes with relatively high closeness and betweenness centrality scores, manifested as the transition from the left posterior regions in the early event-related networks (microstates 1~3) to the right-lateral parietooccipital regions in the networks recruited in the later phases (microstates 4~5). The shift of node centrality in the functional brain networks denotes the switched role of local neural circuits in the coordination of information flows of different cognitive sub-processes.

By using the Louvain method for community detection from large-scale networks (Blondel et al. 2008), all the nodes in the synchronization networks formed in the temporal windows of N170-P200 and P400-700 are parsed into the communities with structurally optimized modularity. Based on the Kamada-Kawai method (Kamada and Kawai 1989), the major community divisions of each event-related network are observed in the force-directed connection graph with an optimized node layout (Fig. 9).

In the temporal networks produced from the three conditions, there are different division patterns and sub-components within the communities. In the early period of the task, the α-band synchronization networks corresponding to N170-P200 under "Ug" and "Tg" conditions can be divided into frontal, premotor-temporal and frontal-parietal-occipital communities in left hemisphere (Fig. 9A), and the β-band networks mainly contain frontal-temporal-parietal and left-lateral temporal-parietal and parietal-occipital communities (Fig. 9B). However, in this period the α-band network organized in "Sc" condition is constituted by left frontal-parietal-occipital and premotor-temporal-parietal communities, with rather sparse inter-node connections and less interconnectivity (Fig. 9A), while the β-band synchronization network can be partitioned into frontal and parietal-occipital and left temporal-parietal communities (Fig. 9B).

In the later period of the task, *i.e.*, the temporal window of P400-700, it can be found that α-band synchronized activities in bilateral frontal-parietal and left frontal-temporal-parietal communities dominate the dynamic networking process of discrete brain areas. Specifically, there are additional functional divisions in α-band networks formed under "Sc" condition, involving left frontal, right frontal-temporal, and right temporal-parietal communities (Fig. 9A). In addition, β-band synchronization networks in "Ug" and "Tg" conditions can be divided into frontal-parietal, frontal-temporal and left temporal-parietal communities, while that in "Sc" condition particularly contains a frontal-temporal community at right cortical hemisphere (Fig. 9B).

3.4 Identifiable EEG channels with time-dependent WPLI differences

In the periods of N170-P200 and P400-700 responses, the WPLI differences between task conditions show time-dependent changes with the adaptive network reorganization (Fig. 10). While compared with α-band WPLIs formed in "Sc" condition, higher synchronizations during the period of N170-P200 are distributed among left temporal, parietal and occipital nodes in the networks under "Ug" and "Tg" conditions. Conversely, in the later neural response process, "Sc" condition elicits higher α-band synchronized activities in right frontal-parietal, frontal-temporal, temporal-parietal and parietal-occipital regions, but evokes fewer activities in left IFG, as compared to "Ug" and "Tg" conditions (Fig. 10A). In β-band functional connectivity microstates (Fig. 10B), there are slightly higher WPLIs in "Ug" and "Tg" conditions than those in "Sc" condition during the N170-P200 period. By contrast, "Sc" condition elicits relatively increased synchronizations in the temporal window of P400-700 than the other two conditions. On the other hand, the comparison performed between the two usual actions reveals that, while subtracting synchronized activities under "Ug" condition, "Tg" condition only evokes more synchronizations in bilateral premotor-parietal areas in N170-P200 period. However, the differences in connection strengths of individual nodes between "Ug" and "Tg" events are not significant in terms of the paired Student's t-tests ($p>0.05$), regardless of the functional connectivity microstates in the earlier (N170-P200) or the later (P400-700) period of the task (Fig. 10A and 10B).

Following the topological transformation of the event-related functional connectivity microstates, EEG electrodes T7, P2 and FP2 with the connection strengths changed from N170-P200 to P400-700 time windows are the distinguishable network nodes in recognizing usual and unintelligible action intentions (Fig. 11). Within the α-band functional networks, T7 at left temporal lobe, P2 at right superior parietal lobe and FP2 on right PFC are found having relatively high accuracies (0.6~0.8) in the classifications of "Ug vs. Sc" and "Tg vs. Sc" task conditions, whereas there are lower accuracies (<0.6) of the individual nodes within the β-band phase-synchronized networks in recognizing the distinctions between task conditions. The identifiability of individual nodes at the left temporal and right superior parietal brain regions is attributed to the differences between task conditions in the α-band temporal-parietal connectivity involved in the earlier N170-P200 period. The right prefrontal node distinguishable in understanding different types of action intentions is related with the α-band frontal-temporal and frontal-parietal connectivity varying in the later cognitive process of P400-700 response (Fig. 10A).

4. Conclusion and Discussion

Based on the ERP brain microstates, phase-synchronized networks organized for different information processing stages of action intention understanding have been constructed, in which complex functional interactions among brain areas are mutually modulated by different cognitive sub-processes and the type of action intention. Moreover, the comparative analysis of DFC has discovered different adaptive reorganization patterns of functional brain networks in the intention identification of distinct action kinematics, manifested as enhanced/suppressed topological configuration of the early event-related network formed in N170-P200 period but the subsequent less/greater reorganization toward the functional network in P400-700 response while understanding usual/unintelligible actions.

N170-P200 and P400-700 responses to action perception and intention inference: By using the CENA method, this study extracts five consecutive brain microstates comprising the ERP components over the task course. Combining the psychological processing mechanism with difference waveforms and source localization, the N170-P200 microstate is most likely indicative of the mirror matching process that acquires information from the actor's action kinematics, and the P400-700 microstate conveys information related to higher-level mentalizing process, at least to the onset of mentalization, which infers the goals/intentions from the actor's hand movement.

At the early stage, the initial small negative N70 in microstate 1 is an early component of visual evoked potential (VEP), primarily located at the occipital cortex. The time interval has been suggested as the onset of discriminative information of action intentions (Ortigue et al. 2009). Since there are no significant differences among the perceived action kinematics, the N70 microstate might be uncorrelated with physical properties of visual input. Microstate 2 (P120) and microstate 3 (N170-P200) have been found to be generated by the same brain sources, and suggested as the sequential neural activities involved in perception of visual materials (Ortigue et al. 2009; Yang et al. 2011). Especially in the microstate 3, the occipitotemporal N170 is a non-specific, motion-related component originating from quinary visual cortex/middle temporal area (V5/MT) while P200 around the parietooccipital region is known to be sensitive to physical properties of visual stimuli (Yamasaki et al. 2012). The cortical source currents corresponding to N170-P200 are mostly distributed in the premotor cortex, anterior IPS, and STS in left cerebral hemisphere (Fig. 4), which have been recognized as the important brain areas critically involved in the mirror system to decode immediate goals of actions (Becchio et al. 2012; Van Overwalle and Baetens 2009). More importantly, the time point where the waveforms for different kinematics start to differ is the timing of the N170-P200 microstate (Fig. 3), indicative of higher sensitivity for physical properties of visual stimuli in the action observation-execution matching process. Specifically, significant potential differences in N170-P200 between task conditions are consistently located in left-lateral brain areas, mainly including the premotor cortex and the STS underlying mirror neuron properties and posterior parietooccipital regions associated with visual processing (Fig. 5C-5E).

At the later stage, the elicited P300 (P3a) in the microstate 4 covering frontal-parietal-temporal cortices is believed to reflect attention allocation and memory updating related to cognitive tasks. The late positive going waveform P400-700 (P3b) in the microstate 5 shows striking event-related activations in the mPFC, ACC and right TPJ (Fig. 4), which have been suggested as the core regions to constitute the mentalizing system (Becchio et al. 2012; Brass et al. 2007; Liew et al. 2011; Van Overwalle and Baetens 2009). Moreover, remarkable disassociation in P3b amplitudes is found among "Ug", "Tg" and "Sc" conditions (Fig. 3). The sources of difference waves between task conditions focus on right-lateral anterior cortical areas to a great extent, primarily including right IFG, STS and anterior temporal lobe and the mPFC (Fig. 5C-5E), some parts of which are thought to be devoted to mentalizing process (Carrington and Bailey 2009). Previous studies have generally suggested that P3b reflects central cognitive processes occurring with the active detection of an attended stimulus and appears related to subsequent memory processing (Polich 2007). Specifically, P3b amplitude depends on the demands for cognitive capacity. Subjectively improbable events will elicit a P3b, and the less probable the event, the larger the P3b amplitude (Donchin 1981; Polich 2007). In line with this conclusion, the highest P3b amplitude has been elicited by "Sc" among the three conditions. In addition to some difference currents in left cerebral hemisphere, understanding unintelligible action in "Sc" condition has evoked extra greater local field potential activities located at right cortical regions compared to "Ug" and "Tg" conditions (Fig. 5C and 5D). As a part of frontal area known to have mirror neuron properties, the right IFG with increased activities is more critical for understanding the intentions behind action observation (Lacoboni et al. 2005; Ortigue et al. 2009, 2010). More importantly, there are concurrently strengthened activities in the mPFC, right STS, and anterior temporal pole, which can be closely associated with inferential processes of actions, particularly unusual actions (Brass et al. 2007; Ortigue et al. 2009).

In previous studies, the ranges of response time of action intention understanding are diverse in different experiments, which might be influenced by action type, task difficulty, and the context of action execution, *etc* (Van der Cruyssen et al. 2009). The identified time interval around 200 ms of microstate 3 is a typical choice of mirror response by most studies (Catmur 2015; Cavallo et al. 2014; Naish et al. 2014; Van der Cruyssen et al. 2009; Vistoli et al. 2015). Besides, the timing of microstate 5 (324~700 ms) shows a high overlap with the time interval of intention inference in the studies using tasks with the same intention identification difficulty (Ortigue et al. 2009, 2010), and keeps the consistency with the suggestion that the response latency of P3b represents the information processing time or time needed to recognize and categorize an unusual event in discriminating oddball and common stimulus (Donchin et al. 1978; Johnso and Donchin 1978). Especially in terms of the source distribution of ERP difference waves, the spatiotemporal shift from left hemisphere dominance in action observation to right hemisphere dominance in intention inference is greatly in line with a large amount of neuroimaging studies (Brass et al. 2007; Catmur 2015; Liew et al. 2011; Ortigue et al. 2009, 2010; Spunt et al. 2011; Van Overwalle and Baetens 2009).

Event-related functional connectivity microstates in α frequency band: The time-frequency analysis of phase lock among trials shows that the ITC in the α frequency band remains significant up to 700 ms, *i.e.*, the maximum time of ERP response in this task, and the β-band ITC is partly involved in the early time window as well (Fig. 2). Over the task course, the functional connectivity of both α- and β-band networks adaptively changes with the ERP-indexed neurocognitive functions, with more significant between-conditions differences in global topology and local nodes revealed in α-band functional networks.

Previous studies have suggested that α-band oscillation is related to highly specific perceptual, attentional and memory processes, and β-band oscillation is mainly associated with motor activity and also plays a role in attentional or other higher cognitive function (Sauseng and Klimesch 2008). Moreover, EEG/ERP studies have pointed out that α-band phase reset particularly contributes to the generation of ERPs, and α phase synchronization is a manifestation of event-related timing mechanism of interactive cortical processing (Hanslmayr et al. 2007; Klimesch et al. 2007). As with the previous suggestions, in this study the ITC in α frequency band demonstrates strong phase-locked activities at ERP component latencies, especially the N170, P300 and P400 response time. By contrast, β-band ITC is more obvious in the earlier period before 200 ms, reflecting the phase-locked oscillations in the β frequencies strongly related with visual perception of motor activity (Fig. 2).

Due to more exact timing of the cognitive sub-processes indexed by ERPs, the α-band functional connectivity microstates isolated in the specific temporal windows probably convey more explicit event-related information of mirroring matching and intention inference of the action intention understanding task. As a result, the α-band functional networks exhibit definite hub centrality changes from the AON to the MZN and reflect the distinguishable features of phase synchronizations between action intention conditions in this study (Fig. 6-11).

Adaptive reconfiguration from left-lateral action observation network to bilateral mentalizing network: Given the timing of the ERP microstates, the analyses on global topology and local node centrality of functional brain networks have discovered two distinctly different structures organized by phase-synchronized oscillations of N170-P200 and P400-700 responses, salient in the α frequency band. The topological change indicates the functional switching of the brain from the AON to the MZN through timely adaptive network reconfiguration.

In "Ug" and "Tg" conditions, the AONs from N170-P200 responses with better configuration for perceptual information processing than that in "Sc" condition are composed of left frontal, premotor-temporal and frontal-parietal-occipital communities (Fig. 9), with functionally centralized nodes located at left premotor, temporal and inferior parietal cortices (Fig. 8). In the AON structure, the premotor cortex plays an important role in identifying the goals or intentions through a direct matching process. The anterior IPS is involved in the on-line motor control of body-part movements for goal objects (*e.g.*, grasping a cup), and the execution and observation of goal-oriented movements. The STS contains polysensory neurons responding to motion from different perceptual modalities, and outputs information to the anterior IPS and premotor cortex (Becchio et al. 2012; Catmur 2015; Ortigue et al. 2009; Rizzolatti et al. 2001; Van Overwalle and Baetens 2009; Woodward and Gerson

2014).

During P400-700 period in "Sc" condition, the MZN structure is more beneficial for inferential information management. Except for bilateral frontal-parietal and temporal-parietal synchronizations, the MZN formed in "Sc" condition contains additional involvement of right frontal and frontal-temporal communities. In the MZN structure, bilateral fronto-parietal synchronizations underlie fundamental cognitive control process, and temporal-parietal synchronizations are most crucial for the representation of goals and intentions in the mentalizing system (Becchio et al. 2012; Van Overwalle and Baetens 2009). In the additionally involved right frontal area, the PFC is critically involved in reflective reasoning about actions and judgments including goals and intentions (Atique et al. 2011; Ortigue et al. 2009; Van Overwalle and Baetens 2009), right IFG is particularly related to intention recognition, and frontotemporal connectivity facilitates mental activity for executive function and inference.

Complementary effect and causal association between mirror and mentalizing systems: The spatiotemporal evolution of the phase-synchronized networks in understanding different action intentions reflects a functionally complementary effect between the topological configurations of the AON and the MZN. As compared with unintelligible actions, the observation of usual actions ("Ug" and "Tg" conditions) induces higher inter-regional connectivity in left premotor-temporoparietal circuit during the early N170-P200 period when the mirror neuron system is firing, which is consistent with Gardner et al.'s (2015) finding that movement familiarity dynamically modulates more activities in cortical areas of AON. In this experimental task, the enhanced phase synchronization in the AON is a manifestation of increased information communication among task-related brain areas when the observed actions are rather usual in our daily life, *e.g.*, "grasping a cup for drinking" and "grasping a cup for moving". By contrast, in "Sc" condition, the mirror function of the brain is suppressed while the perceived action is outside the observer's repertoire of familiar movements, presented as lower synchronized activities in the AON. However, in the later time window of P400-700 response, the brain areas involved in task-related mentalization become more activated, especially the right frontal, temporal and parietal cortices where there is increasing involvement of right frontal-temporal and temporal-parietal synchronizations under "Sc" condition. During this period, the increased frontal-temporal connectivity can be associated with strengthened inference function for detecting intentionality, and the enhanced temporal-parietal interactions might be responsive for higher effort in estimating the orientation or direction of the behavior in order to predict its possible end-state (or goal) (Becchio et al. 2012; Brass et al. 2007; Van Overwalle and Baetens 2009). The variation in dynamic functional networks supports De Lange et al.'s (2008) finding that part of the mirror-neuron system is only activated in action perception whereas part of the mentalizing system becomes active in the recognition of others' intentions, suggesting distinct but complementary function of the two systems.

The previous studies have been debating whether the mirror and mentalizing systems are mutually independent or cooperated in human understanding of intentionality (Becchio et al. 2012; Catmur 2015; Neal and Kilner 2010; Tidoni and Candidi 2016). Van Overwalle and Baetens (2009) have concluded that neither mirror nor mentalizing system subserves the other, since the two systems are rarely concurrently activated. During performing specific tasks, if brain areas subserving one system are activated while the areas of the other system are inactive, the two systems might be well independent. On the other hand, a substantial number of studies support the assumption that the two systems work together, and mirror neurons might provide rapid and intuitive input to the mentalizing system to support and constrain inferential process (Catmur 2015; Gardner et al. 2015; Tidoni and Candidi 2016; Van Overwalle and Baetens 2009). In this study, the DFC analysis reveals that the AON and the MZN are largely not overlapped in topological structures and show temporally isolated enhancement of functional integration among brain areas, which indicates respective dominant roles in detecting distinct aspects of human behaviors, *i.e.*, action perception and intention inference. Although the AON and the MZN have been recruited in isolation by this specific task, the DFC under different action intention conditions indicates that there is implicit causal association between the recruitment of low-level mirror matching and high-level inference activities. Intention identification of irrational, implausible or unusual action is cognitively more demanding and additionally requires observer's mental effort and cognitive load on working out why it is being performed (Catmur 2015; Van Overwalle 2009; Van Overwalle and Baetens 2009). Previous dynamic network research has demonstrated that mental effort, in particular, can modulate long-distance functional connectivity among anatomically separated brain areas (Bassett et al. 2006; Kitzbichler et al. 2011). As a result, when there is no immediate visual substrate on which to complete intentionality judgments, effortful cognitive processing for indentifying the intentionality of unintelligible action would drive greater topological reorganization toward an enhanced MZN structure with higher global integration and additional involvement of task-related brain areas, and vise versa. Thus, the acquisition of sensorimotor information from the AON can be viewed as a prerequisite of imposing different cognitive workloads on an observer, which restrain or drive functional integration among cortical area of the mentalizing system, with working memory serving as the interface between visual perception and inferential process.

Potential application of the identified EEG/ERP patterns: Intention understanding is a basic requirement for human-machine interaction. Action classification and brain response recognition are two possible ways to understand human intention (Yu et al. 2015). The present study reveals the switched functions of the brain from the AON to the MZN during an action intention understanding task, with the synchronization differences between task conditions changed from left frontal-temporal and temporal-parietooccipital to right frontal-temporal-parietal regions. According to the neurocognitive functions from recognizing action kinematics to inferring intentionality, feature extraction of phase synchrony was conducted on EEG electrodes in the temporal windows of N170-P200 and P400-700 responses. The discrimination results from different methods demonstrate that the time-evolving α-band WPLIs represent identifiable EEG/ERP patterns for understanding usual action and unintelligible action. Particularly, the best classification accuracy in the frequency-specific feature combination from the two temporal windows has been attained at electrode site T7, indicating the adaptiveness of left temporal lobe in the cooperative interaction with task-related neuronal populations that are self-organized in understanding usual and unintelligible action intentions. The EEG sensor-level DFC study provides preliminary evidence for cognitive detection and intention classification in brain-computer interface (BCI) applications that require rapid and reliable extraction of discriminatory information from event-related EEG patterns. According to the justified EEG electrode sites and cognition-related temporal windows, further single-trial classification for individual's action intention recognition is worthy to be systematically explored and improved, such as an effective feature combination from multiple channels with optimized discriminatory information involved in the switched phase relationship from the AON to the MZN. Additionally, an action intention understanding paradigm more appropriate for BCI practice should be considered and developed in the future.

Acknowledgements

This work was supported in part by the National Basic Research Program of China under Grant 2015CB351704, the Natural Science Foundation of China under Grants 31600862 and 61773114, the Key Research and Development Plan (Industry Foresight and Common Key Technology) of Jiangsu Province under Grant BE2017007-3, the Support Program of Excellent Young Talents in Universities of

Anhui Province under Grant gxyqZD2017064, and the Natural Science Foundation of Bengbu Medical College under Grant BYKY1604ZD. The authors would like to thank the anonymous reviewers for their thoughtful comments and suggestions.

References

Atique B, Erb M, Gharabaghi A, Grodd W, Anders S (2011) Task-specific activity and connectivity within the mentalizing network during emotion and intention mentalizing. Neuroimage 55(4): 1899-1911.

Bassett DS, Meyerlindenberg A, Achard S, Duke T, Bullmore E (2007) Adaptive reconfiguration of fractal small-world human brain functional networks. Proc Natl Acad Sci U S A 103(51): 19518-19523.

Becchio C, Cavallo A, Begliomini C, Sartori L, Feltrin G, Castiello U (2012) Social grasping: from mirroring to mentalizing. Neuroimage 61(1): 240-248.

Blakemore SJ, Decety J (2001) From the perception of action to the understanding of intention. Nat Rev Neurosci 2(8): 561-567.

Blondel VD, Guillaume JL, Lambiotte R, Lefebvre E (2008) Fast unfolding of communities in large networks. J Stat Mech-Theory E 2008(10): P10008.

Brass M, Schmitt RM, Spengler S, Gergely G (2007) Investigating action understanding: inferential processes versus action simulation. Curr Biol 17(24): 2117-2121.

Buccino G, Baumgaertner A, Colle L, Buechel C, Rizzolatti G, Binkofski F (2007) The neural basis for understanding non-intended actions. Neuroimage 36: T119-T127.

Bullmore E, Sporns O (2009) Complex brain networks: graph theoretical analysis of structural and functional systems. Nat Rev Neurosci 10(3): 186-198.

Cacioppo S, Cacioppo JT (2015) Dynamic spatiotemporal brain analyses using high-performance electrical neuroimaging, part ii: a step-by-step tutorial. J Neurosci Meth 256: 184-197.

Cacioppo S, Weiss RM, Runesha HB, Cacioppo JT (2014) Dynamic spatiotemporal brain analyses using high performance electrical neuroimaging: theoretical framework and validation. J Neurosci Meth 238: 11-34.

Carrington SJ, Bailey AJ (2009) Are there theory of mind regions in the brain? a review of the neuroimaging literature. Hum Brain Mapp 30(8): 2313-2335.

Carter EJ, Hodgins JK, Rakison DH (2011) Exploring the neural correlates of goal-directed action and intention understanding. Neuroimage 54(2): 1634-1642.

Catmur C (2014) Unconvincing support for role of mirror neurons in "action understanding": commentary on Michael et al. Front Hum Neurosci 8: 553.

Catmur C (2015) Understanding intentions from actions: direct perception, inference, and the roles of mirror and mentalizing systems. Conscious Cogn 36: 426-433.

Cavallo A, Heyes C, Becchio C, Bird G, Catmur C (2014) Timecourse of mirror and counter-mirror effects measured with transcranial magnetic stimulation. Soc Cogn Affect Neurosci 9(8): 1082-1088.

De Lange FP, Spronk M, Willems RM, Toni I, Bekkering H (2008) Complementary systems for understanding action intentions. Curr Biol 18(6): 454-457.

Decety J, Grèzes J (1999) Neural mechanisms subserving the perception of human actions. Trends Cogn Sci 3(5): 172-178.

Delorme A, Makeig S (2004) EEGLAB: an open source toolbox for analysis of single-trial EEG dynamics including independent component analysis. J Neurosci Methods 134:9–21.

Donchin E (1981) Surprise!… surprise?. Psychophysiology 18(5): 493-513.

Donchin E, Ritter W, McCallum WC (1978) Cognitive psychophysiology: the endogenous components of the ERP. Event-Related Brain Potentials in Man 349-411.

Erdös P, Rényi A (1961) On the strength of connectedness of a random graph. Acta Math Hungar 12:261–267.

Gardner T, Goulden N, Cross ES (2015) Dynamic modulation of the action observation network by movement familiarity. J Neurosci 35(4): 1561-1572.

Gramfort A, Papadopoulo T, Olivi E, Clerc M (2010) OpenMEEG: opensource software for quasistatic bioelectromagnetics. Biomed Eng Online 9(1): 45.

Hanslmayr S, Klimesch W, Sauseng P, Gruber W, Doppelmayr M, Freunberger R, et al (2007) Alpha phase reset contributes to the generation of ERPs. Cereb Cortex 17(1): 1-8.

Hutchison RM, Womelsdorf T, Allen EA, Bandettini PA, Calhoun VD, Corbetta M, et al (2013) Dynamic functional connectivity: promise, issues, and interpretations. Neuroimage 80(1): 360-78.

Johnso R, Donchin E (1978) On how P300 amplitude varies with the utility of the eliciting stimuli. Electroencephal Clin Neurophysiol 44(4): 424-437.

Kamada T, Kawai S (1989) An algorithm for drawing general undirected graphs. Inform Process Lett 31(1), 7-15.

Khanna A, Pascualleone A, Michel CM, Farzan F (2014) Microstates in resting-state EEG: current status and future directions. Neurosci Biobehav Rev 49: 105-113.

Klimesch W, Sauseng P, Hanslmayr S (2007) EEG alpha oscillations: the inhibition-timing hypothesis. Brain Res Rev 53(1): 63-88.

Kitzbichler MG, Henson RN, Smith ML, Nathan PJ, Bullmore ET (2011) Cognitive effort drives workspace configuration of human brain functional networks. J Neurosci 31(22): 8259-8270.

Koenig T, Prichep L, Lehmann D, Sosa PV, Braeker E, Kleinlogel H et al (2002) Millisecond by millisecond, year by year: normative EEG microstates and developmental stages. Neuroimage 16(1): 41-48.

Lacoboni M, Molnar-Szakacs I, Gallese V, Buccino G, Mazziotta JC, Rizzolatti G (2005). Grasping the intentions of others with one's own mirror neuron system. PLoS Biol 3(3): e79.

Liew SL, Han S, Aziz-Zadeh L (2011) Familiarity modulates mirror neuron and mentalizing regions during intention understanding. Hum Brain Mapp 32(11): 1986-1997.

Lohmann G, Margulies DS, Horstmann A, Pleger B, Lepsien J, Goldhahn D et al (2010) Eigenvector centrality mapping for analyzing connectivity patterns in fMRI data of the human brain. Plos One 5(4): e10232.

Meyer ML, Spunt RP, Berkman ET, Taylor SE, Lieberman MD (2012) Evidence for social working memory from a parametric functional MRI study. Proc Natl Acad Sci U S A 109(6): 1883-1888.

Milston SI, Vanman EJ, Cunnington R (2013) Cognitive empathy and motor activity during observed actions. Neuropsychologia 51(6): 1103-1108.

Milz P, Faber PL, Lehmann D, Koenig T, Kochi K, Pascual-Marqui RD (2015) The functional significance of EEG microstates-associations with modalities of thinking. Neuroimage 125(104): 643-656.

Marsh LE, Mullett TL, Ropar D, Hamilton AF (2014) Responses to irrational actions in action observation and mentalising networks of the human brain. Neuroimage 103: 81-90.

Naish KR, Houstonprice C, Bremner AJ, Holmes NP (2014) Effects of action observation on corticospinal excitability: muscle specificity, direction, and timing of the mirror response. Neuropsychologia 64: 331-348.

Neal A, Kilner JM (2010) What is simulated in the action observation network when we observe actions? Eur J Neurosci 32(10): 1765–1770.

Opsahl T, Agneessens F, Skvoretz J (2010) Node centrality in weighted networks: generalizing degree and shortest paths. Soc Netw 32(3): 245-251.

Ortigue S, Sinigaglia C, Rizzolatti G, Grafton ST (2010) Understanding actions of others: the electrodynamics of the left and right hemispheres. A high-density EEG neuroimaging study. Plos One 5(8): e12160.

Ortigue S, Thompson JC, Parasuraman R, Grafton ST (2009) Spatio-temporal dynamics of human intention understanding in temporo-parietal cortex: a combined EEG/fMRI repetition suppression paradigm. Plos One 4(9): e6962.

Polich J (2007) Updating P300: an integrative theory of P3a and P3b. Clin Neurophysiol 118(10): 2128-2148.

Rizzolatti G, Fogassi L, Gallese V (2001) Neurophysiological mechanisms underlying the understanding and imitation of action. Nat Rev Neurosci 2(9): 661-670.

Rubinov M, Sporns O (2010) Complex network measures of brain connectivity: uses and interpretations. Neuroimage 52(3): 1059-1069.

Sauseng P, Klimesch W (2008) What does phase information of oscillatory brain activity tell us about cognitive processes? Neuroscience and biobehavioral reviews 32(5): 1001-13.

Sporns O, Honey CJ, Kötter R (2007) Identification and classification of hubs in brain networks. Plos One 2(10): e1049.

Spunt RP, Satpute AB, Lieberman MD (2011) Identifying the what, why, and how of an observed action: an fMRI study of mentalizing and mechanizing during action observation. J Cogn Neurosci 23(1): 63-74.

Spunt RP, Lieberman MD (2013) The busy social brain: evidence for automaticity and control in the neural systems supporting social cognition and action understanding. Psychol Sci 24(1): 80-86.

Tadel F, Baillet S, Mosher JC, Pantazis D, Leahy RM (2011) Brainstorm: a user-friendly application for MEG/EEG analysis. Comput Intell Neurosci 2011: 8.

Tidoni E, Candidi M (2016) Commentary: understanding intentions from actions: direct perception, inference, and the roles of mirror and mentalizing systems. Front Behav Neurosci 10(185): 13.

Van der Cruyssen L, Van Duynslaeger M, Cortoos A, Van Overwalle F (2009) ERP time course and brain areas of spontaneous and intentional goal inferences. Soc Neurosci 4(2): 165-184.

Van Overwalle F (2009) Social cognition and the brain: a meta-analysis. Hum Brain Mapp 30(3): 829-858.

Van Overwalle F, Baetens K (2009) Understanding others' actions and goals by mirror and mentalizing systems: a meta-analysis. Neuroimage 48(3): 564-584.

Van Overwalle F, Van den Eede S, Baetens K, Vandekerckhove M (2009) Trait inferences in goal-directed behavior: ERP timing and localization under spontaneous and intentional processing. Soc Cogn Affect Neurosci 4(2): 177-190.

Vinck M, Oostenveld R, Wingerden MV, Battaglia F, Pennartz CMA (2011) An improved index of phase-synchronization for electrophysiological data in the presence of volume-conduction, noise and sample-size bias. Neuroimage 55(4): 1548-1565.

Virji-Babul N, Moiseev A, Cheung T, Weeks D, Cheyne D, Ribary U (2010) Spatial-temporal dynamics of cortical activity underlying reaching and grasping. Hum Brain Mapp 31(1): 160-171.

Vistoli D, Passerieux C, El Zein M, Clumeck C, Braun S, Brunet-Gouet E (2015) Characterizing an ERP correlate of intentions understanding using a sequential comic strips paradigm. Soc Neurosci 10(4): 391-407.

Woodward AL, Gerson SA (2014) Mirroring and the development of action understanding. Philos Trans R Soc B Biol Sci 369(1644): 20130181.

Yamasaki T, Muranaka H, Kaseda Y, Mimori Y, Tobimatsu S (2012) Understanding the pathophysiology of alzheimer's disease and mild cognitive impairment: a mini review on fMRI and ERP studies. Neurol Res Int 2012: 719056.

Yang Y, Gu G, Guo H, Qiu YH (2011) Early event-related potential components in face perception reflect the sequential neural activities. Acta Physiol Sinica 63(2): 97-105.

Yu Z, Kim S, Mallipeddi R, Lee M (2015) Human intention understanding based on object affordance and action classification. In IEEE International Joint Conference on Neural Networks 1-6.

Figure legends

Fig. 1 Experimental paradigm of "hand-cup interaction" observation task. (A) Three hand-cup interaction actions: a hand grasping a cup for using it (Ug); a hand grasping a cup for moving it (Tg); a hand touching a cup without any obvious purpose (Sc). (B) Timeline of stimulus presentation and time interval of an epoch of EEG data.

Fig. 2 Time-frequency diagrams of inter-trial coherence of principle components at left and right hemispheres. (A) "Ug" (B) "Tg" and (C) "Sc" conditions.

Fig. 3 Grand average of ERPs for the three conditions (*i.e.*, Ug, Tg, and Sc) from channels FZ, CZ, PZ and POZ. Time=0 corresponds to the onset of "hand-cup interaction" presentation. The figures show that each condition has elicited five ERP components that are marked with vertical dotted lines. The blue, green, and red solid lines represent the "Ug", "Tg", and "Sc" conditions respectively.

Fig. 4 Brain microstates and cortical sources activated in the task course, illustrated by EEG data averaged across subjects from the "Ug" condition. Top: EEG in "Ug" condition; Middle: five electric field topologies corresponding to the GFP peaks in EEG duration; Bottom: absolute values of source currents of microstates displayed on MRI viewer and cortical surface.

Fig. 5 Topological maps of GFP and difference waves. Top: brain mapping of (A) N170-P200 microstate and (B) P400-700 microstate in "Ug", "Tg" and "Sc" conditions. Bottom: source current distribution of difference waves on the cortical surface (R: right side; L: left side). The electrodes on the brain maps represent the locations with significant differences in (C) "Sc-Ug", (D) "Sc-Tg", and (E) "Tg-Ug" via the paired t-tests with FDR correction.

Fig. 6 WPLI-based functional microstate networks under the "Ug", "Tg" and "Sc" conditions during continuous temporal windows of ERPs. (A) α and (B) β frequency bands. The functional connections are constructed by setting a fixed threshold for each association matrix. The color marked in an EEG electrode represents "degree" of the node in a network, with the value indicated in the color bar.

Fig. 7 Temporal evolution of global topology of the WPLI-based functional networks under the "Ug", "Tg" and "Sc" conditions. (A) α and (B) β frequency bands. Top: measures of connection density and characteristic path length in the five microstates; Bottom: statistical results from the paired t-tests between each two conditions for measures of connection density and characteristic path length in the five microstates, with * indicating $p<0.05$. The blue, green and red curves and bars represent "Ug", "Tg" and "Sc" conditions respectively.

Fig. 8 Topological distributions of node centrality in five functional connectivity microstates: (A) α and (B) β frequency bands. From top to bottom: distribution of nodes with high degree centrality, closeness centrality, and betweenness centrality by selecting the nodes with the highest centrality scores (top 10 from each type of centrality) and further excluding the nodes with too low scores. The electrodes colored in blue, green and red represent the centralized nodes of "Ug", "Tg", and "Sc" conditions respectively.

Fig. 9 Force-directed node layouts and major communities of the functional connectivity microstates in the temporal windows of N170-P200 and P400-700 responses. (A) α and (B) β frequency bands. From top to bottom: "Ug", "Tg" and "Sc" conditions. Each node corresponds to an EEG electrode, and the colors represent different functional communities parsed by the Louvain method.

Fig. 10 WPLI differences between task conditions of the functional connectivity microstates in the temporal of N170-P200 and P400-700 responses. (A) α and (B) β frequency bands. From top to bottom: the networks are constructed by the difference values of WPLIs from "Ug minus Sc", "Tg minus Sc", and "Tg minus Ug". The blue edges indicate increased synchronized node pairs (*i.e.,* positive difference values), and the red edges represent decreased synchronizations (*i.e.*, negative difference values). The width of an edge is proportional to the absolute difference value in comparison. The colored nodes refer to significant difference in connection strength (paired Student's t-tests with a FDR correction: $p<0.05$), and the color of a node is proportional to its log p in the paired t-test, with the value indicated in the color bar.

Fig. 11 Feature distributions and discrimination results for node connection strengths in the temporal windows of N170-P200 and P400-700 responses. EEG electrodes (A) T7 at the left temporal lobe, (B) P2 at the right superior parietal lobe and (C) FP2 on the right prefrontal cortex. Top: the scattergram of subject-based samples. The horizontal axis represents the connection strength of an electrode in the temporal window of N170-P200 and the vertical axis P400-700. The blue, green and red markers represent the samples from the "Ug", "Tg", and "Sc" task conditions respectively. Bottom: discrimination accuracy between each two task conditions from

LDA, SVM and Naive Bayes. The outliers in the red circles are excluded from the discriminant analysis according to the fuzz c-means clustering method.

Table 1 Duration and cortical sources of event-related microstates

Figure 1

Click here to download Figure fig1.tiff

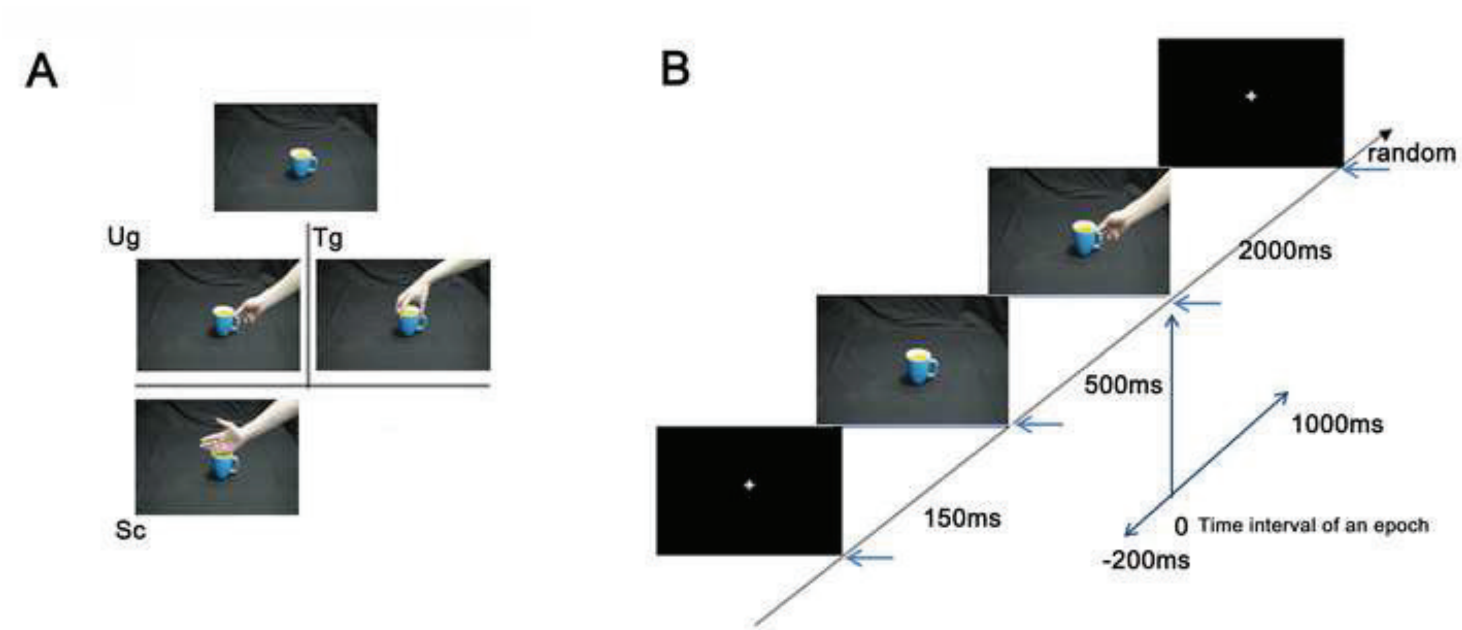

Figure 2 Click here to download Figure Fig2.tiff

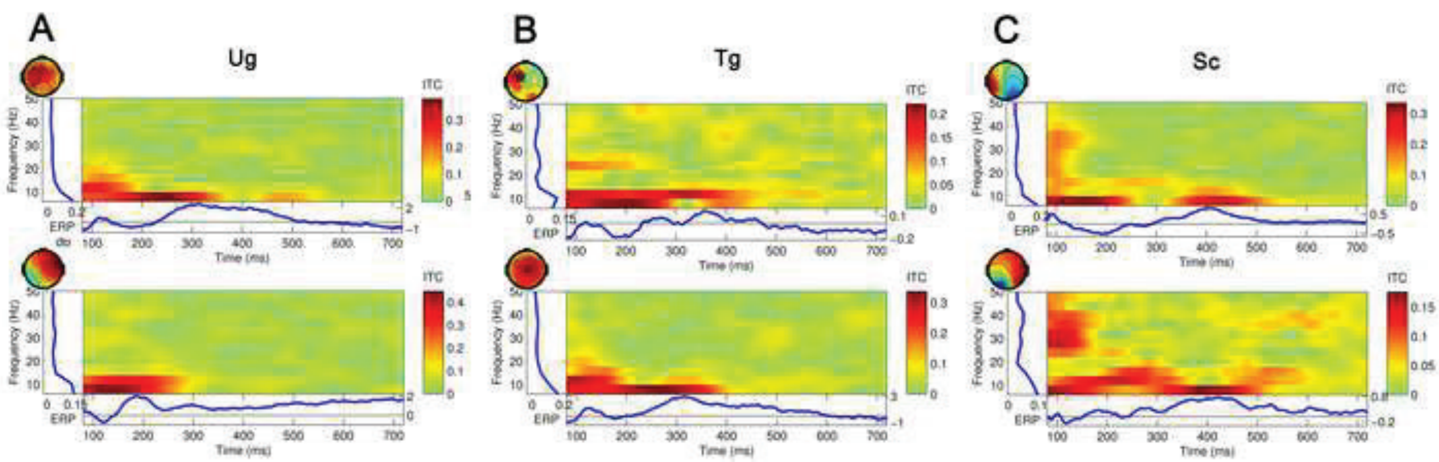

Figure 3

Click here to download Figure Fig3.tiff

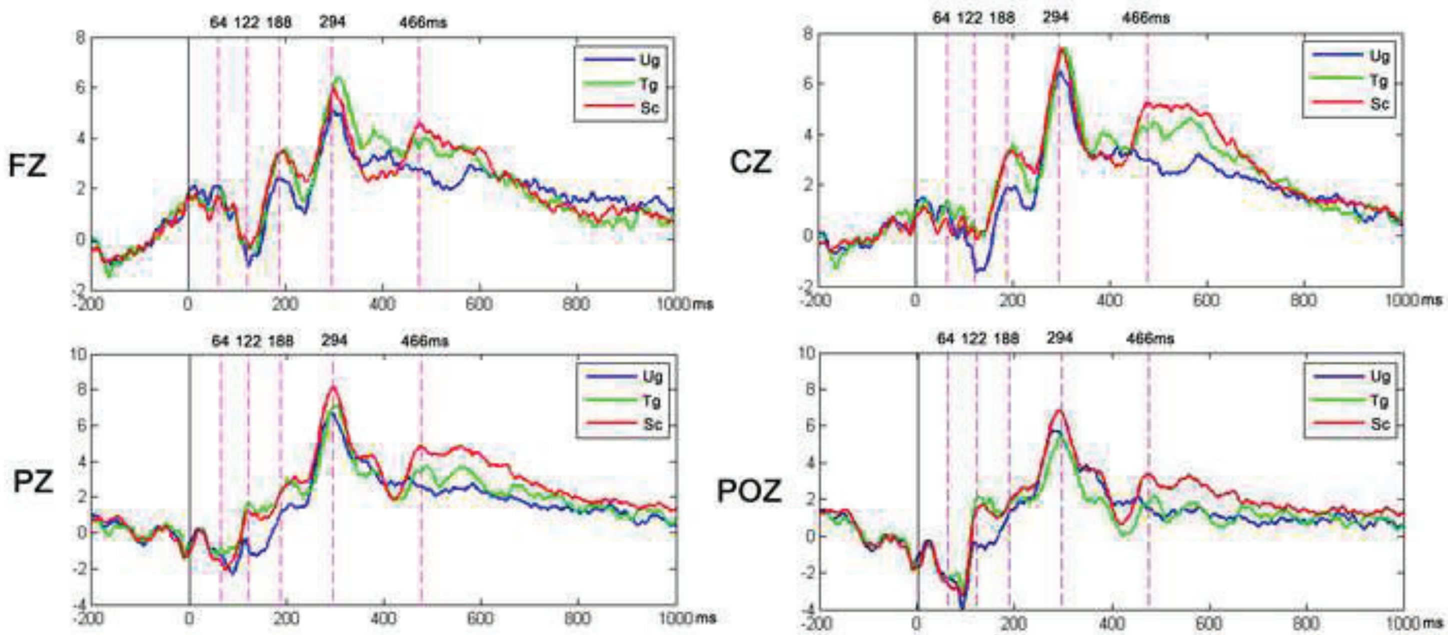

Figure 4

Click here to download Figure Fig4.tiff

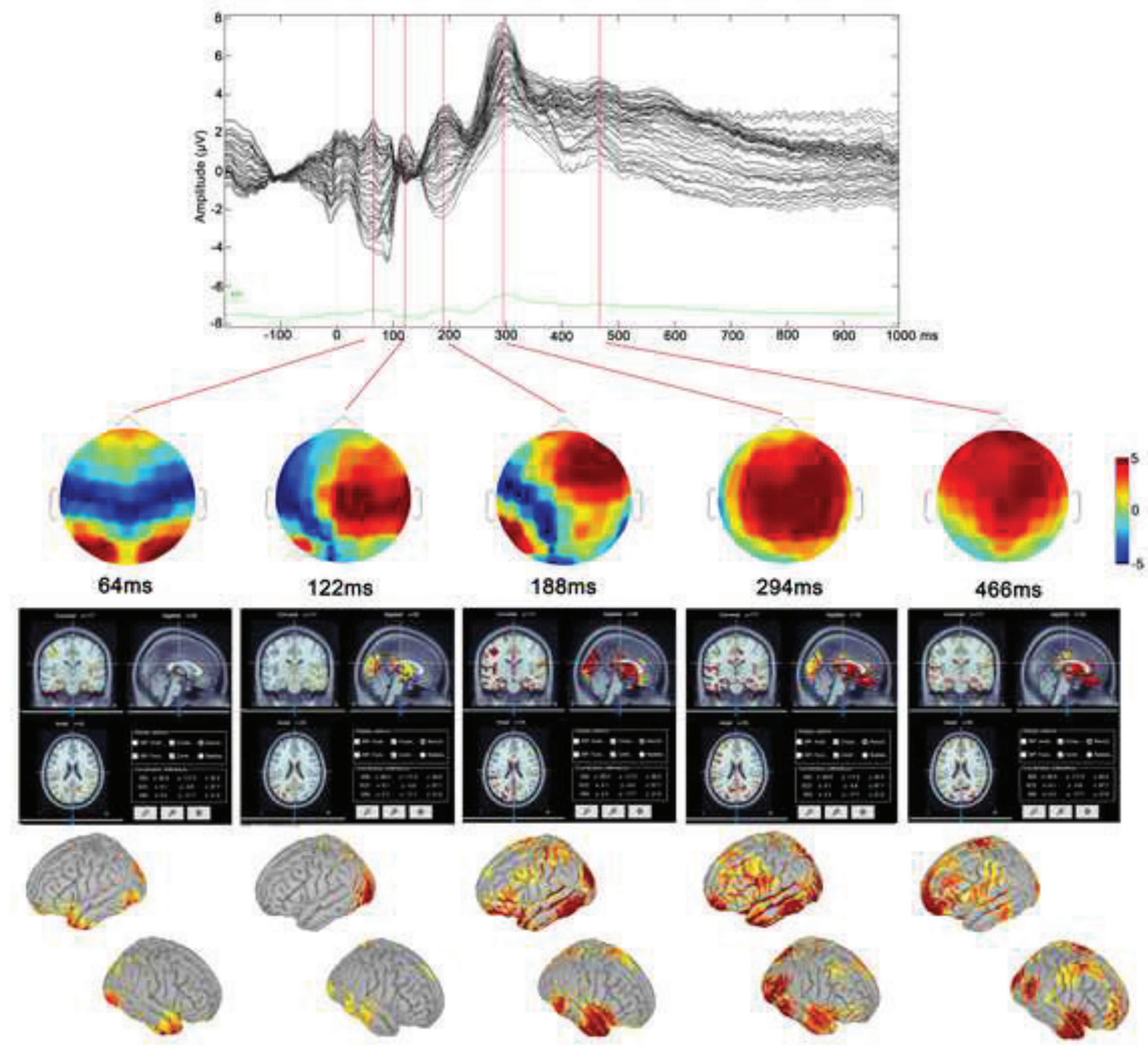

Figure 5

Click here to download Figure Fig5.tiff

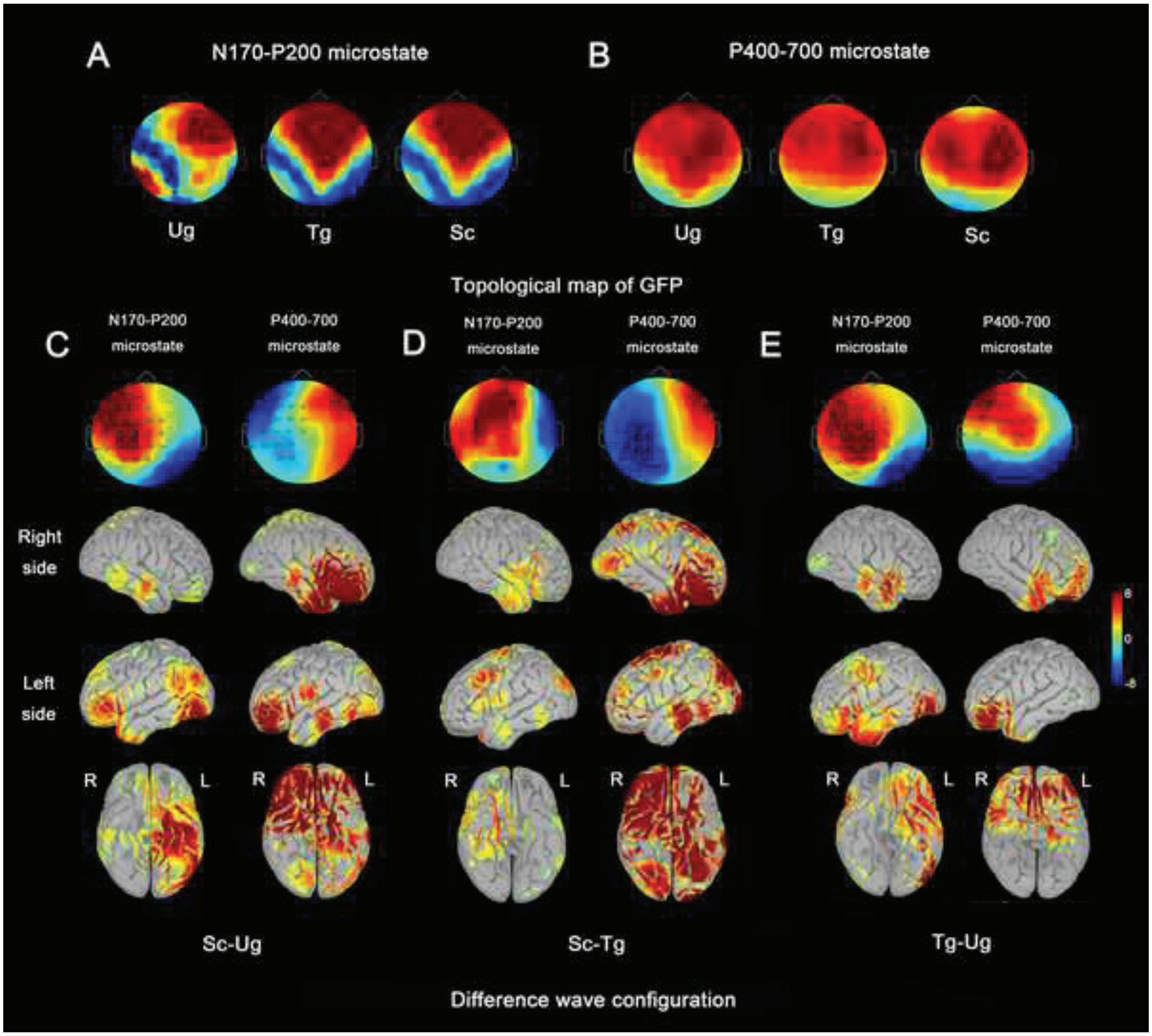

Figure 6 Click here to download Figure Fig6.tiff

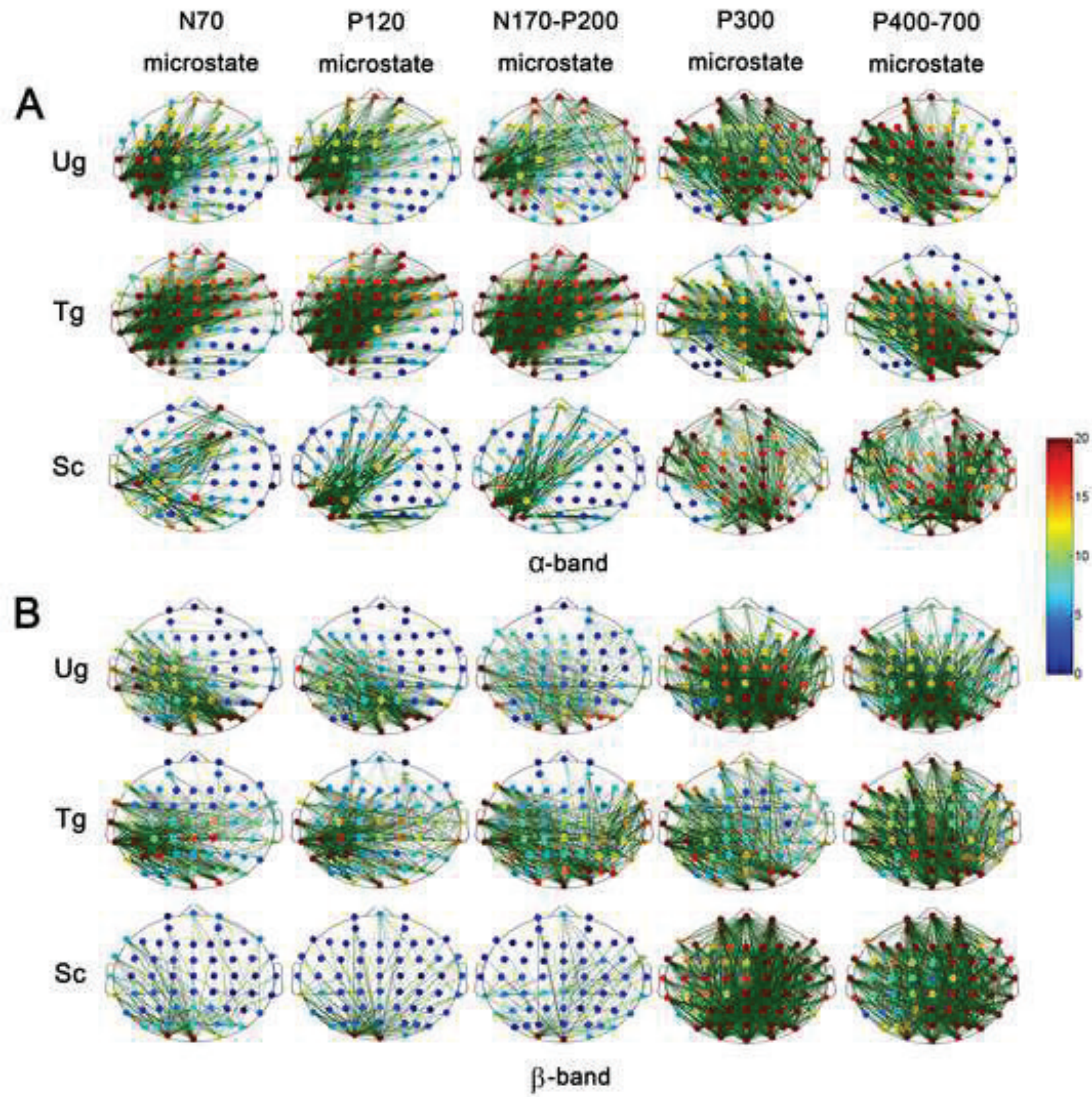

Figure 7

Click here to download Figure Fig7.tiff

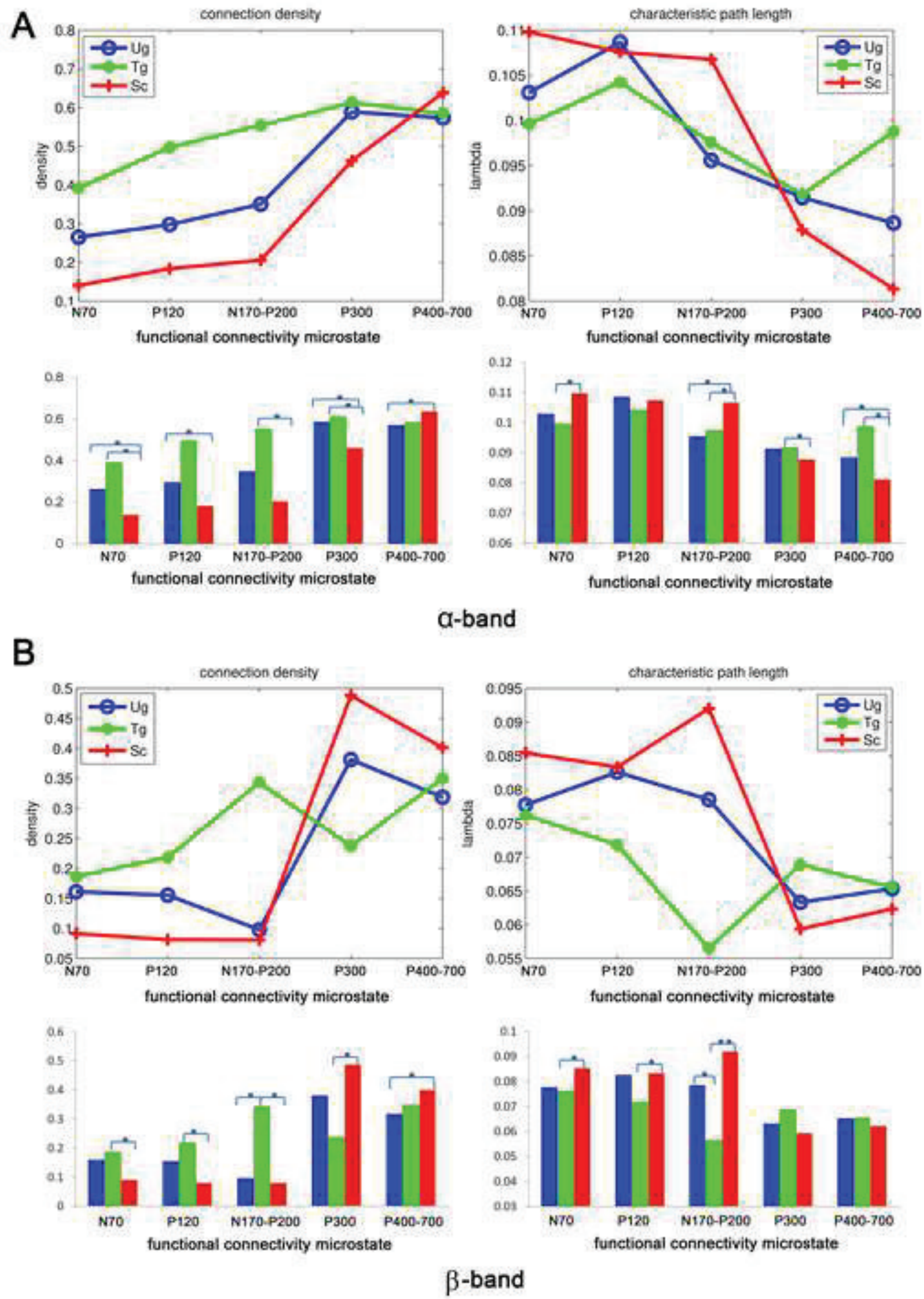

Figure 8

Click here to download Figure Fig8.tiff

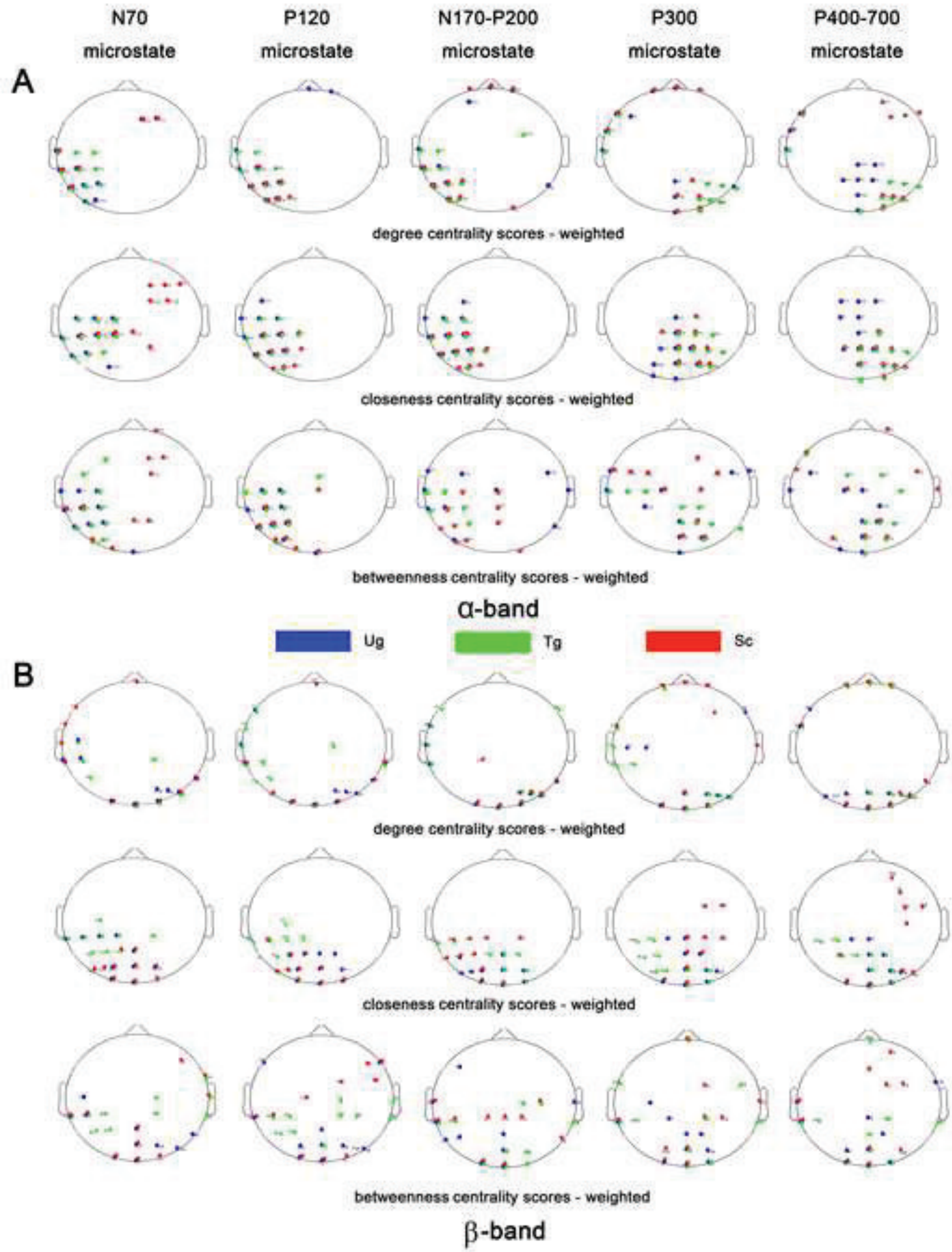

Figure 9 Click here to download Figure Fig9.tiff

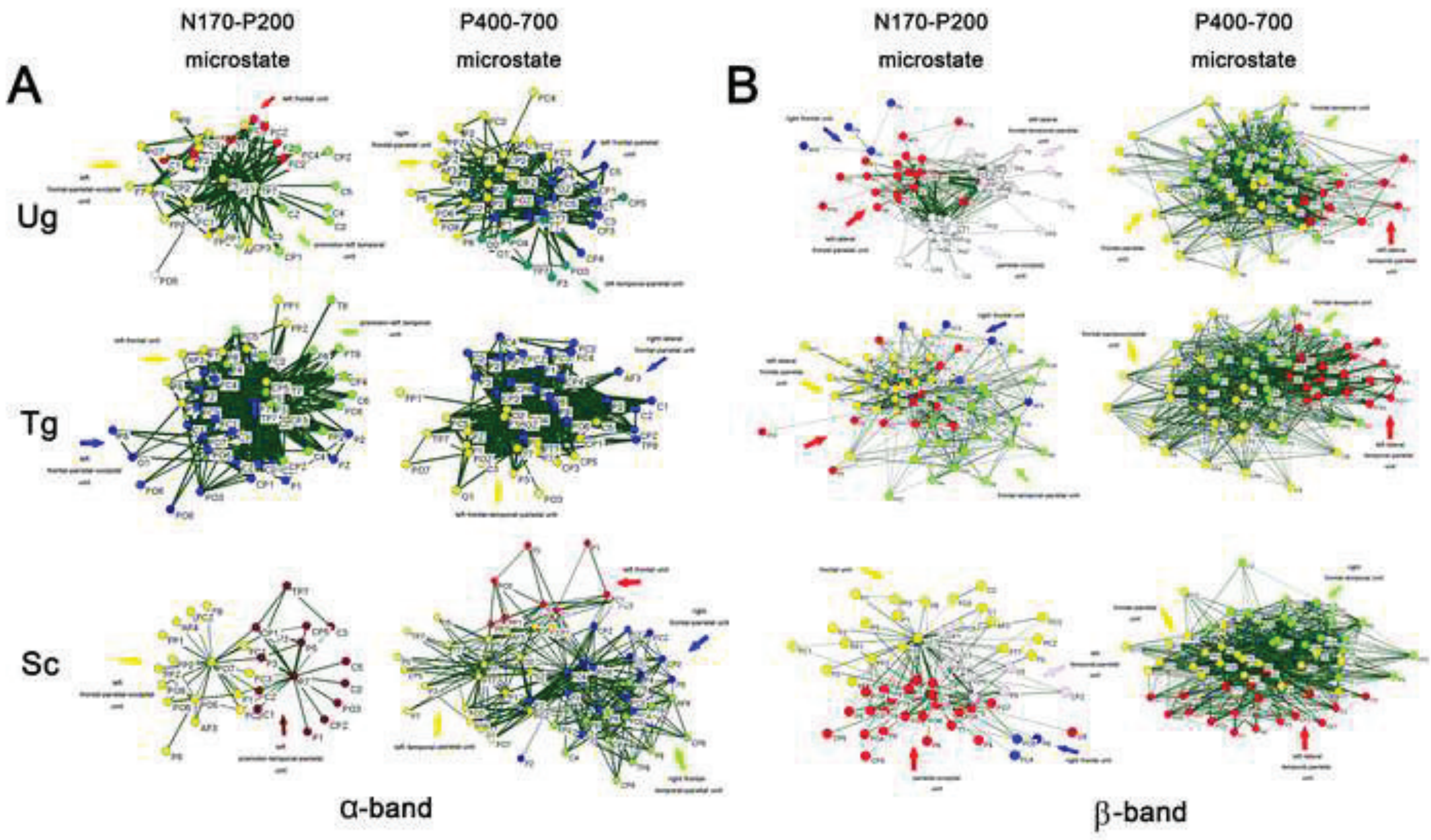

Figure 10

Click here to download Figure Fig10.tiff

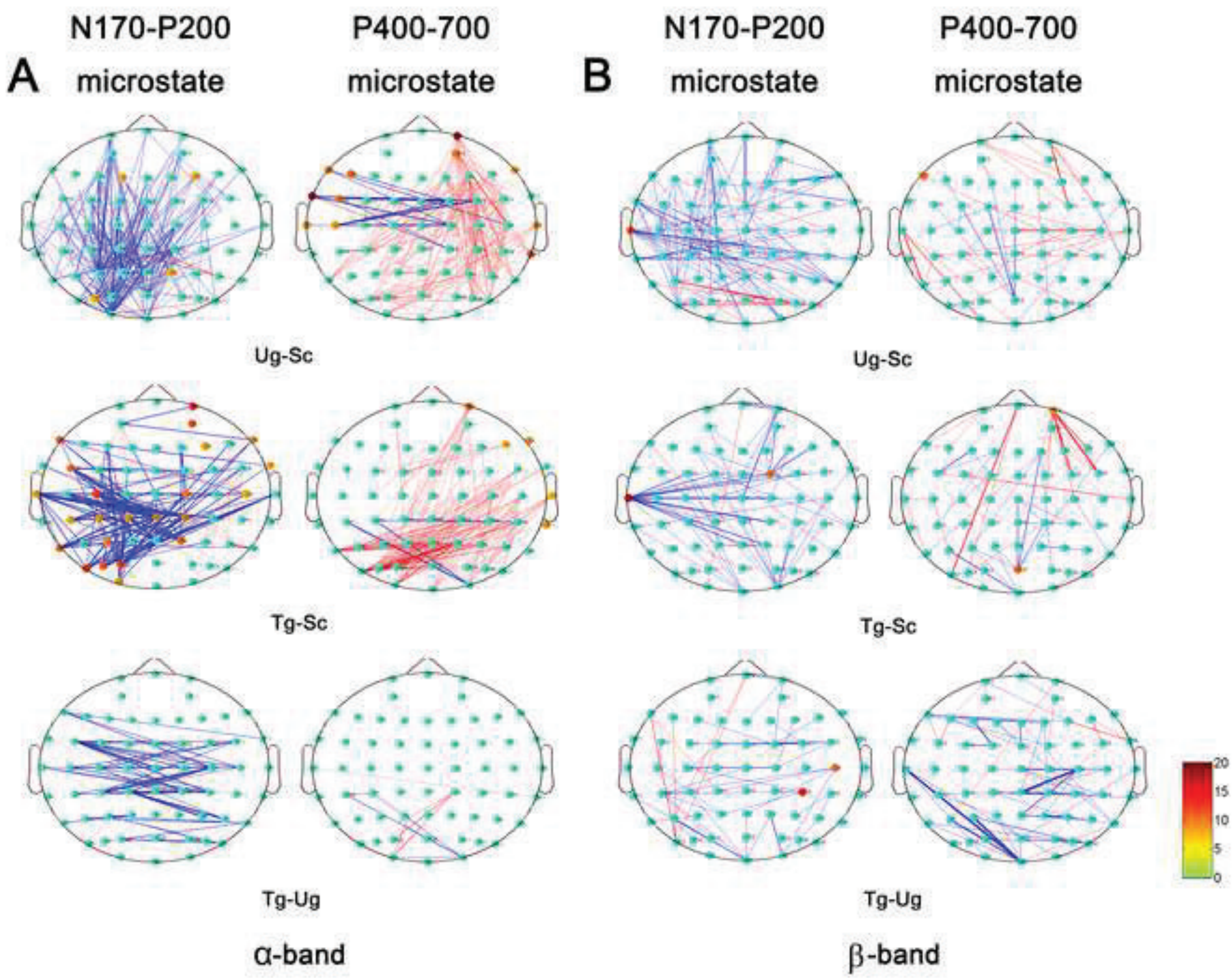

Figure 11

Click here to download Figure Fig11.tiff

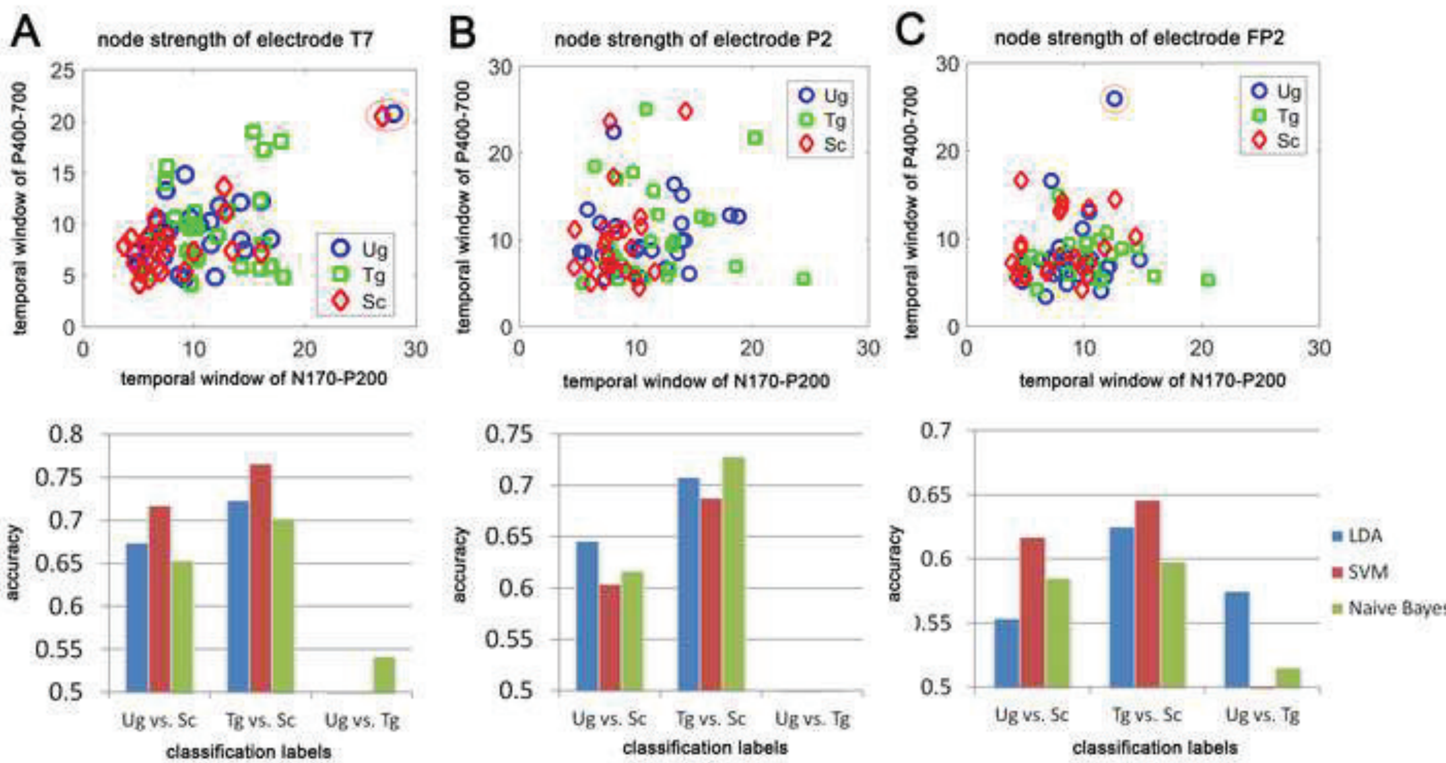

Table 1

Table 1 Duration and cortical sources of event-related microstates

Event-related microstates		microstate 1	microstate 2	microstate 3	microstate 4	microstate 5
ERP component		N70	P120	N170-P200	P300	P400-700
Duration (ms)	Ug	0~94	106-146	164~234	254~312	326~700
	Tg	0~96	106~146	158~258	270~318	330~700
	Sc	0~80	106~150	156~248	274~320	326~700
Cortical sources		occipital cortex	left-lateral parietal and occipital cortices	left-lateral anterior intraparietal sulcus, premotor cortex, superior temporal sulcus, and parietooccipital cortex	anterior cingulate, temporal lobe, parietooccipital cortex and right-lateral temporoparietal cortex	medial prefrontal cortex, anterior cingulate, superior temporal sulcus, right-lateral anterior temporal pole and temporoparietal cortex